Check for updates

AGU ADVANCING EARTH AND SPACE SCIENCES

Geophysical Research Letters

RESEARCH LETTER
10.1029/2024GL110845

Distribution, Mixing, and Transformation of a Loop Current Ring Waters: The Case of Gulf of Mexico

Mathieu Gentil[1,2], Enric Pallàs-Sanz[1], Leo Middleton[3], Angel Ruiz-Angulo[4], Thomas Meunier[1,3,5], Giovanni Durante[1], Miguel Tenreiro[1], Sheila N. Allis Estrada[1], and Julio Sheinbaum[1]

[1]Center for Scientific Research and Higher Education at Ensenada, Ensenada, Mexico, [2]Now at Aix-Marseille University, Université de Toulon, CNRS, IRD, MIO UM 110, Marseille, France, [3]Woods Hole Oceanographic Institution, Woods Hole, MA, USA, [4]Institute of Earth Sciences, University of Iceland, Reykjavik, Iceland, [5]Laboratoire d'Océanographie Physique et Spatiale (LOPS), University of Brest, CNRS, IRD, Ifremer, IUEM, Brest, France

Abstract Mesoscale warm-core rings, known as Loop Current rings (LCRs) reshape the Gulf of Mexico water masses by redistributing large amounts of heat and salt laterally. LCRs also transform water masses via diapycnal mixing, but the mechanisms by which this occurs are poorly measured. Here, we present glider-MicroPod turbulence observations that reveal enhanced mixing below the mixed layer, along the eddy edges, driving the LCR's heat, salt, and oxygen exchanges. Interleavings of adjacent water masses may be interpreted mainly as a manifestation of submesoscale processes through stirring of the spice gradients, which facilitates double-diffusive mixing that transforms Subtropical Underwater into Gulf Common Water. Our findings highlight the need for ocean models to parameterize double-diffusive mixing processes directly resulting from submesoscale tracer stirring, which may be important at basin scale in the presence of LCRs in the Gulf of Mexico.

Plain Language Summary In the Gulf of Mexico (GoM), anticyclonic eddies, known as Loop Current rings (LCRs) carrying warm and salty water shape the basin's water mass properties, which in turn, affects the regional climate and marine life. The water mass properties are altered by turbulent mixing. However, the mechanisms leading to the mixing of GoM waters are still under debate due to a lack of observations. Here, we use an autonomous underwater vehicle (glider) equipped with a turbulence sensor to assess the nature of LCR mixing and its impact on water properties. The breaking of internal waves in the ocean is often thought to be responsible for turbulent mixing in the ocean interior. However, our findings demonstrate that a process called double-diffusive convection is responsible, where turbulence is forced by differences between the temperature and salinity of adjacent water parcels. We found that double-diffusive convection was the main driver in mixing heat, salt, and oxygen along the eddy edges, producing Gulf Common Water. These findings highlight the need to include double diffusive processes in ocean models for more accurate simulations.

Key Points:

- Direct observations of turbulence reveal the distribution of mixing across a Gulf of Mexico Loop Current Ring
- Subtropical Underwater is transformed into Gulf Common Water through double-diffusive convection on the edges of the eddy

Supporting Information:

Supporting Information may be found in the online version of this article.

Correspondence to:

M. Gentil,
mathieu.gentil@mio.osupytheas.fr

Citation:

Gentil, M., Pallàs-Sanz, E., Middleton, L., Ruiz-Angulo, A., Meunier, T., Durante, G., et al. (2024). Distribution, mixing, and transformation of a Loop Current Ring waters: The case of Gulf of Mexico. *Geophysical Research Letters*, *51*, e2024GL110845. https://doi.org/10.1029/2024GL110845

Received 20 JUN 2024
Accepted 24 OCT 2024

© 2024. The Author(s).
This is an open access article under the terms of the Creative Commons Attribution-NonCommercial-NoDerivs License, which permits use and distribution in any medium, provided the original work is properly cited, the use is non-commercial and no modifications or adaptations are made.

1. Introduction

Loop Current rings (LCRs) are energetic mesoscale anticyclonic eddies, which transport large amounts of warm and salty Subtropical Underwater (SUW) through the Gulf of Mexico (GoM). These waters are characterized by significant thermohaline anomalies, up to ∼10°C and more than 1 psu (Meunier et al., 2018). Because of their large heat and salt content, LCRs influence significantly the GoM's watermass properties (Vidal et al., 1994; P. Hamilton et al., 2018; Meunier et al., 2020), hurricane intensification (Jaimes et al., 2016; John et al., 2023; Shay et al., 2000), sea level rise (Thirion et al., 2024), and biogeochemical cycles (Damien et al., 2021; Linacre et al., 2019). Understanding the processes that control the transformation and variability of LCRs water masses is of climatic and biogeochemical relevance.

As they drift westward through the GoM, LCR waters undergo significant transformations due to surface heat fluxes, river discharge, evaporation, precipitation, as well as isopycnal and diapycnal mixing (P. Hamilton et al., 2018). Recent observations indicate that Ekman buoyancy fluxes may be one of the main drivers of LCRs decay, by converting their available potential energy into kinetic energy (Meunier et al., 2024). Kinetic energy is then dissipated through the action of wind stress work, instabilities and turbulent mixing (Brannigan, 2016; Herring, 2010; Meunier et al., 2024; Pérez et al., 2022; Sosa-Gutiérrez et al., 2020). Mixing is likely mediated by

19448007, 2024, 23, Downloaded from https://agupubs.onlinelibrary.wiley.com/doi/10.1029/2024GL110845 by Ifremer Centre Bretagne Blp, Wiley Online Library on [09/12/2024]. See the Terms and Conditions (https://onlinelibrary.wiley.com/terms-and-conditions) on Wiley Online Library for rules of use; OA articles are governed by the applicable Creative Commons License

submesoscale (1–10 km) processes, which have been observed along the edge of LCRs (Molodtsov et al., 2020) but are too small to be observed by altimetry (Meunier et al., 2020).

Ultimately, water mass properties are irreversibly mixed at the dissipation scale ($\sim$1 cm−1m). However, different turbulent processes (e.g., shear production and double-diffusion) are associated with different vertical turbulent fluxes between water masses (Kunze, 2003). In shear-driven turbulence, some of the input turbulent kinetic energy (TKE) turns into turbulent dissipation, while some acts in breaking the stratification. In this framework, temperature and salinity are assumed to be mixed vertically with the same effective diffusivity as the buoyancy. Below the mixed layer, vertical shear is mainly attributed to geostrophic currents and internal waves (Fernández-Castro et al., 2020; Martínez-Marrero et al., 2019; Pallàs-Sanz et al., 2016; Pollard et al., 1973; Wu et al., 2015). Alternatively, in double-diffusive convection (DDC), potential energy is converted into TKE, which is then dissipated, and temperature and salinity have differing effective diffusivities. Although previously considered primarily a feature of less active regions, such as the Arctic, recent evidences have shown that double-diffusively unstable stratifications can develop due to the interleaving of water masses via stirring of submesoscale structures (Fine et al., 2022; Sanchez-Rios et al., 2024). This argument was extended by Middleton et al. (2021), who suggested that sub-km stirring could result in DDC at the overturning scale. An outstanding question araises as to the role and contribution of DDC to the LCR's water transformation.

Molodtsov et al. (2020) suggested that the interleaved features along the edge of LCRs were intrusions, similar to those found in the Arctic (Bebieva & Timmermans, 2016), whose dynamics are governed by micro-scale molecular diffusion (B. B. Ruddick & Richards, 2003). However, Meunier et al. (2019) and Shcherbina et al. (2009) argued that layering and thermohaline interleaving may be created by lateral stirring. Vertically differential lateral stirring of density-compensating temperature and salinity anomaly may induce a direct variance cascade (Meunier et al., 2015), possibly down to the overturning scales where DDC may become important.

Here, we present direct turbulence observations in an early life-stage LCR drifting through the GoM (the most intense phase of eddy energy decay identified by Meunier et al. (2024)). We use data collected from a ship survey as well as glider observations, to quantify the turbulent mechanisms of LCR's water mass transformation and assess their importance in comparison with the finescale parameterization of double-diffusion. We show that Middleton et al. (2021)'s parameterization provides dissipation rates along the eddy's edge that are consistent with our direct observations. The eddy's turbulent structure is presented, and its variability is discussed within the limitations of the data set. DDC is identified as a key contributor to Subtropical Underwater heat and salt content erosion leading to Gulf Common Water (GCW) production, highlighting the importance of accurate parameterization in ocean models to understand the formation of water masses in the Gulf of Mexico.

2. Data and Methods

2.1. Overview of the Experiment

As part of the PhytBloomEddy project (“Phytoplankton Blooms in a Loop Current Eddy”), a multi-platform survey was performed to measure physical and biogeochemical properties within, and at the periphery of a recently detached LCR, named ”Yazoo” (Woods Hole Group; https://www.horizonmarine.com/loop-current-eddie).

During a 7-day ship survey in November 2022, microstructure profiles were collected using a vertical microstructure profiler 6,000 to estimate turbulent dissipation rates. Turbulent data collection was limited to the LCR's west side due to equipment loss. Simultaneously, CTD profiles were gathered using a *Sea-Bird SBE 19 plus* probe. Finally, a Seaglider surveyed the northern edge of the LCR (Figure 1a), capturing data with horizontal and vertical resolutions of 1 km and 1 m, respectively. The Seaglider was equipped with a *Rockland Scientific MicroPod*, an unpumped *Seabird CTD Sail* probe, and an Anderaa-4831F oxygen sensor. The Seaglider's average speed during deployment was approximately 0.2 m s^{-1}, and the FP07 fast-response temperature sensor of the *MicroPod* sampled at 512 Hz with an effective resolution of 10 milliseconds.

Conservative temperature, absolute salinity, potential density anomaly, buoyancy frequency, and spice were computed through the TEOS-10 Gibbs Seawater Oceanographic toolbox (McDougall & Barker, 2011). Spice and dissolved oxygen were high-pass filtered using a second-order Butterworth filter with a cutoff scale of 80 m, following (Meunier et al., 2015). Mean profiles for the LCR and Gulf waters were derived by averaging CTD data

10.1029/2024GL110845

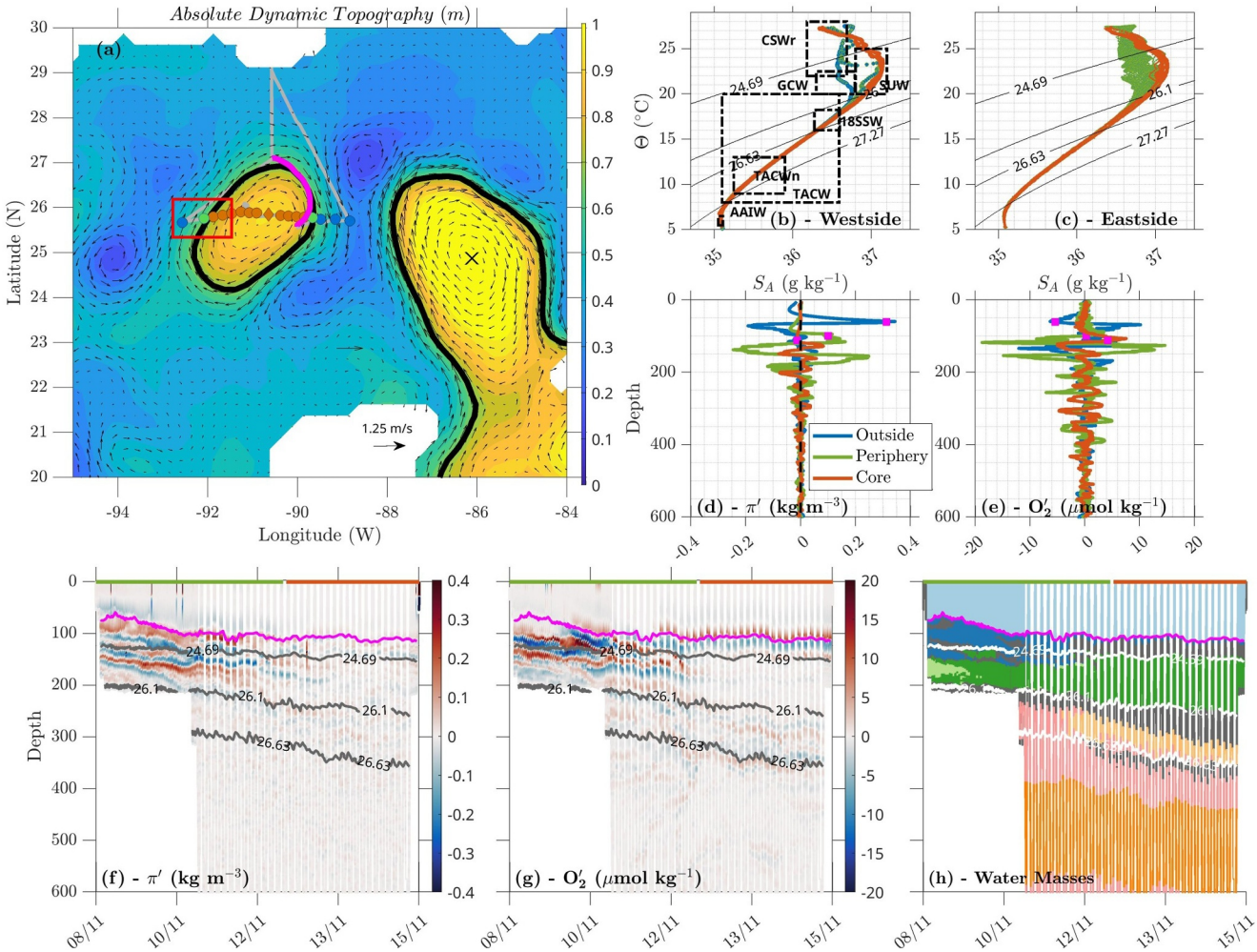

Figure 1. (a) Map of absolute dynamic topography from AVISO averaged between November 7 and 17, 2022. The gray line indicates the ship trajectory, colored circles show CTD stations across the Loop Current Ring (LCR), and red square the vertical microstructure profiler measurements. The black outline indicates the eddy's and Loop Current's contour, and the pink line, the azimuthal Seaglider section. Figures 1f–1h are derived from Seaglider data. (b) and (c) Conservative temperature - absolute salinity (Θ - S_A) diagrams from R/V Pelican and glider sampling, respectively. Green, blue, and orange dots (lines in (d), (e), (f), (g), and (h)) represent eddy's outside, periphery, and center, respectively. The dashed boxes are Θ - S_A limits of the water masses (colored in (h)), according to the Portela et al. (2018) clasification: CSWr (Caribbean Surface Water remnant - dark blue), GCW (Gulf Common Water - light green), SUW (Subtropical UnderWater - dark green), 18SSW (18°C Sargasso Sea Water - light orange), and TACW (Tropical Atlantic Central Water - pink) and its core (TACWn - dark orange). To complement in (h), light blue and dark gray are the Surface Mixed Layer and the Transtion Layers, respectively. Spice (d), (f) and dissolved oxygen (e), (g) anomalies for eastside (f), (g) and westside (d), (e) eddy location. Magenta square (d), (e) and lines (f), (g), (h) represent the mixed-layer depth.

(Figure S1 in Supporting Information S1). The LCR's periphery was characterized by wiggling temperature-salinity profiles between GCW and SUW (Figure 1b). AVISO daily absolute dynamic topography was used to detect and track the LCR, following the methodology of Chaigneau et al. (2008) as modified by Sosa-Gutiérrez et al. (2020) (Figure 1a).

2.2. Microstructure and Turbulence Parameters

Frequent adjustment of the glider's flight along the eddy edge resulted in significant platform vibration. Frajka-Williams et al. (2022), showed that microstructure temperature-based estimates of the dissipation rate, ε, are less contaminated by platform vibration; therefore we focused on the T-S estimates of ε. The temperature-based ε, may be estimated by determining the Batchelor wavenumber, defined by $k_B = (1/2\pi)\left(\varepsilon/\nu D_T^2\right)^{1/4}$, and inverting to yield

19448007, 2024, 23, Downloaded from https://agupubs.onlinelibrary.wiley.com/doi/10.1029/2024GL110845 by Ifremer Centre Bretagne Blp, Wiley Online Library on [09/12/2024]. See the Terms and Conditions (https://onlinelibrary.wiley.com/terms-and-conditions) on Wiley Online Library for rules of use; OA articles are governed by the applicable Creative Commons License

$$\varepsilon = \nu D_T^2 (2\pi k_B)^4, \tag{1}$$

where ν is the kinematic viscosity of seawater, and $D_T = 1.44 \times 10^{-7}$ m^2 s^{-1} is the molecular diffusivity coefficient of temperature. We determined k_B by fitting a theoretical Batchelor spectrum (Batchelor, 1959) to the observed power spectra of temperature gradients, using the MATLAB toolbox (https://github.com/bscheife/turbulence_temperature) (Scheifele et al., 2018), based on the theoretical framework of B. Ruddick et al. (2000) and Peterson and Fer (2014). Dissipation of thermal variance rate (χ) is computed from spectral fits as detailed in supplementary material (see Text S1 and Figure S2 in Supporting Information S1). Power spectrum densities of temperature gradients were estimated from 10-s sections of data (with total of 5,120 points), using fast Fourier transform (FFT) on 4-s segments; each spectral point was based on four FFT segments with 50% overlapping.

The eddy diffusivity, κ_z, is inferred from measurements of ε following the Osborn (1980) model:

$$\kappa_z = \Gamma \frac{\varepsilon}{N^2}, \tag{2}$$

where Γ is the mixing coefficient and represents the efficiency of transforming TKE into potential energy and is classically assumed to be 0.2 in the shear-driven regime (Osborn, 1980). Then vertical turbulent heat, salt, and oxygen fluxes, Q_h (W m^{-2}), Q_S (kg m^{-2} s^{-1}), and Q_{O_2} (mmol m^{-2} s^{-1}), respectively, can be computed from κ_z.

$$Qh = -\rho c_p \kappa_z \frac{\partial T}{\partial z}, \tag{3}$$

$$Q_S = \frac{1}{1000}\left(-\rho \kappa_z \frac{\partial S}{\partial z}\right), \tag{4}$$

$$Qo_2 = -\kappa_z \frac{\partial [O_2]}{\partial z}, \tag{5}$$

Where, ρ is density, c_p is the specific heat capacity of seawater, and $\frac{\partial T}{\partial z}$, $\frac{\partial S}{\partial z}$, $\frac{\partial [O_2]}{\partial z}$ are the vertical gradients of potential temperature, absolute salinity and oxygen concentration, respectively. However in DDC (e.g., salt-finger or diffusive-convection), turbulence is driven by the release of potential energy so that the shear-production term of the TKE budget may become negligible and the mixing coefficient can be assumed to be close to -1 (Laurent & Schmitt, 1999). The subsequent vertical turbulent fluxes of heat and salt may not be estimated with a single constant diffusivity.

To help differentiating DDC from turbulent processes, we used the buoyancy Reynolds number (Gargett, 1988)

$$Re_b = \frac{\epsilon}{\nu N^2}. \tag{6}$$

When Re_b is less than 10, shear-driven turbulence is suppressed by stratification and the resulting buoyancy flux is also suppressed (Bouffard & Boegman, 2013; Ivey et al., 2008; Shih et al., 2005; Stillinger et al., 1983). For large Re_b, the effective turbulent diffusivities for heat and salt become the same (Jackson & Rehmann, 2014). Therefore, we use Re_b to distinguish between DDC and shear-driven turbulence.

Identifying double-diffusive favorable conditions via the density ratio R_ρ is a technique used by many authors (Oyabu et al., 2023; Schmitt, 1994; Washburn & Käse, 1987; Yang et al., 2016), however, the scale at which R_ρ should be measured to infer instability is an important factor. Middleton et al. (2021) suggested that the overturning scale is the relevant scale at which the density ratio must be double-diffusively favorable to force instability, which is usually significantly smaller than the resolution used to calculate R_ρ. In this study, the overturning scale is 0.17 m, estimated using the Ozmidov length scale, as shown in supplementary material (Figure S3 in Supporting Information S1). Also, they argue that the stirring of compensated thermohaline variance (spice) along isopycnals can lead to double-diffusively favorable R_ρ values on sub-measurement scales. Using this argument, they developed a parameterization for double-diffusive buoyancy fluxes as the result of the

19448007, 2024, 23, Downloaded from https://agupubs.onlinelibrary.wiley.com/doi/10.1029/2024GL110845 by Ifremer Centre Bretagne Blp, Wiley Online Library on [09/12/2024]. See the Terms and Conditions (https://onlinelibrary.wiley.com/terms-and-conditions) on Wiley Online Library for rules of use; OA articles are governed by the applicable Creative Commons License

19448007, 2024, 23, Downloaded from https://agupubs.onlinelibrary.wiley.com/doi/10.1029/2024GL110845 by Ifremer Centre Bretagne Blp, Wiley Online Library on [09/12/2024]. See the Terms and Conditions (https://onlinelibrary.wiley.com/terms-and-conditions) on Wiley Online Library for rules of use; OA articles are governed by the applicable Creative Commons License

stirring motions. The computation of ϵ from this method is detailed in supplementary material, and applied to the glider section. We include the possibility that a background doubly stable stratification may still support double-diffusive convection due to lateral stirring by using only the buoyancy Reynolds number to distinguish between double-diffusive and shear-driven regimes. This is supported by the results of Middleton et al. (2021).

To compute the DDC-induced heat and salt fluxes, we cannot use a single turbulent diffusivity, so we use the methodology of J. M. Hamilton et al. (1989). Assuming the validity of Osborn and Cox (1972) relationship between heat flux and dissipation of thermal variance χ, and the Osborn (1980) relationship between dissipation rate and buoyancy flux $\epsilon\,\Gamma = \langle w'b' \rangle$, J. M. Hamilton et al. (1989) derived the relationship:

$$\gamma = \frac{\alpha \langle w'T' \rangle}{\beta \langle w'S' \rangle} \approx \frac{\Gamma R_\rho \Sigma^{DDC}}{R_\rho \Sigma^{DDC} - \Gamma(R_\rho - 1)}, \tag{7}$$

where $\langle\rangle$ is the mean operator between isopycnal layers, $R_\rho = \frac{\alpha \frac{\partial T}{\partial z}}{\beta \frac{\partial S}{\partial z}}$ is the density ratio, α and β are the thermal expansion and haline contraction coefficients, respectively. $\Sigma^{DDC} = \frac{\chi N^2}{2\epsilon\left(\delta\tilde{\theta}/\delta z\right)^2}$ is a scaled dissipation ratio defined by J. M. Hamilton et al. (1989). The turbulent diffusivities of temperature (κ_T) and salinity (κ_S) could then be estimated from the dissipation rate and the above expression for γ.

$$\kappa_T = \frac{\left\langle w'T' \right\rangle}{\left\langle \theta_z \right\rangle} = \frac{\langle \epsilon \rangle}{g\alpha\Gamma(1-\gamma^{-1})\langle \theta_z \rangle}, \tag{8}$$

$$\kappa_S = \frac{\left\langle w'S' \right\rangle}{\left\langle S_z \right\rangle} = \frac{\langle \epsilon \rangle}{g\beta\Gamma(\gamma-1)\langle S_z \rangle}, \tag{9}$$

where $\Gamma = -1$, when double-diffusive convection occurs, and $\Gamma = 0.2$ when shear-driven mixing occurs. In DDC, diffusivities for density are associated with up-gradient flux, while those for heat and salt are down-gradient but opposite to buoyancy fluxes. Here, oxygen flux is assumed to be down-gradient. The molecular diffusivity of oxygen (2×10^{-9} m^2 s^{-1}; Ferrell & Himmelblau, 1967) and salinity (1×10^{-9} m^2 s^{-1}; Vitagliano & Lyons, 1956) are similar, suggesting that turbulent diffusivity for oxygen behaves similarly to that of salinity. Therefore, κ_S from Equation 9 is replaced by κ_ρ in Equation 5 under DDC-favorable conditions. Note that if shear-driven mixing dominates, at high buoyancy Reynolds number the effective diffusivities of temperature and salinity are equal, so $\gamma = R_\rho$.

To summarize the procedure, we first categorized the water column into shear- and DDC-favorable conditions. As both double diffusion and shear-driven turbulence can drive diapycnal mixing (B. R. Ruddick et al., 2010; Fine et al., 2018, 2022), we chose to consider the distribution of ϵ as a function of the buoyancy Reynolds number and the density ratio to highlights their importance in the mixing. For shear-favorable conditions, we use κ_z from Osborn (1980) model to compute turbulent fluxes from Equations 3–5. In DDC-favorable conditions, we used κ_T and κ_S from the DDC expressions (Equations 8 and 9).

2.3. Water Mass Definition and Analysis

The mixed layer depth was defined based on a change in density of 0.125 kg m^{-3} from a reference depth of 10 m (Monterey & Levitus, 1997). Water masses were characterized according to the criteria of conservative temperature (θ), absolute salinity (S_A), and dissolved oxygen concentration $[O_2]$ as defined by Portela et al. (2018). To assess the transformation of LCR's water, we employed the optimal multiparameter analysis (Tomczak Jr, 1981; Tomczak & Large, 1989), using θ, S_A, $[O_2]$, and potential vorticity. The latter was computed following Pérez et al. (2022) for glider observations, with noise reduction techniques for vertical derivatives as suggested by Tomczak (1999). For each observation, optimal multiparameter analysis attempts to solve a constrained linear system using the method of least squares fitting to find the mixing coefficients. The mixing coefficients account for the contribution of each source water type to the sample. Water mass types are identified as (quasi) continuous trajectories in the parameter space based on typical T-S diagrams included in the supplementary material (Figure

19448007, 2024, 23, Downloaded from https://agupubs.onlinelibrary.wiley.com/doi/10.1029/2024GL110845 by Ifremer Centre Bretagne Blp, Wiley Online Library on [09/12/2024]. See the Terms and Conditions (https://onlinelibrary.wiley.com/terms-and-conditions) on Wiley Online Library for rules of use; OA articles are governed by the applicable Creative Commons License

S1 in Supporting Information S1). Optimal multiparameter analysis was applied only in the pycnocline waters (i.e., between 8 and ∼28°C) excluding the mixed layer and the plume-influenced waters, since the method requires avoiding sources and sinks.

3. Results

3.1. LCR's Water Masses Distribution

The LCR is evident in Figure 1a as a circular patch of high absolute dynamic topography, with a radius of ∼150 km centered at 26°N - 91°W. Figure 1h shows a vertical section of the water mass distribution along the glider trajectory. Caribbean surface water remnants (CSWr) is evident between the surface and the 24.69 kg m^{-3} isopycnal, which represents the boundary between the mixed layer and the SUW salinity maximum. The CSWr thickness exhibits spatial variability, reaching 60 m near the eddy's periphery, transitioning into a thin layer of 20 m within the eddy center (Figure 1h).

Within the eddy, the SUW core is found between the 24.69–26.1 kg m^{-3} isopycnals (∼130–200 m), with a salinity maximum reaching 37.3 g kg^{-1}. This contrasts with the surrounding GCW outside the eddy, where salinity is lower (36.5 g kg^{-1}; Figure 1b). Between these water masses, the $\Theta - S_A$ diagram alternates between SUW and GCW. The glider mission focused on the eddy's boundary to capture this complexity in greater details (Figure 1c). The high-resolution observations reveal distinct layers of spice anomaly (up to 20 m thick), characterized by alternating signs and amplitudes reaching 0.25 kg m^{-3} (Figure 1f). Remarkably, similar patterns are observed in the distribution of dissolved oxygen anomaly (Figure 1g), reaching −20 μmol kg^{-1}, closely aligned with the spice anomaly layers, highlighting the strong link between thermohaline properties and oxygen distribution.

For densities larger than 26.1 kg m^{-3} (>220 m), the Θ-S_A diagram do not show distinctive features between Gulf's and LCR's water (Figure 1b). Along this isopycnal, where Tropical Atlantic Central Water (TACW), 18°C Sargasso Sea Water (18SSW), and a transitional layer interact (Figure 1h), spice and oxygen anomaly layers with opposite signs are also observed, but 4 to 5 times weaker than those in shallower regions (Figures 1f and 1g). These stacks of thermohaline and biogeochemical layers of alternating signs, evident in glider data in the north east of the eddy, are also shown by CTD casts (Figures 1d and 1e).

3.2. Diapycnal Mixing: Distribution, Variability and Origin

High-resolution observations in the LCR reveal significant vertical variability in ϵ, with values ranging from 10^{-12} to 10^{-7} W kg^{-1} (Figure 2a). While we observe values as low as 10^{-12} W kg^{-1}, we focus our analysis on regions where ϵ is greater than 10^{-10} W kg^{-1}, as lower values are typically below the threshold for meaningful mixing. Enhanced turbulent mixing is observed within the mixed-layer, as expected by wind, wave and convective effects. However, subsurface regions exhibit distinct zones of elevated ϵ $\left(O\left(10^{-9}/10^{-8}\right)\mathrm{W\,kg^{-1}}\right)$, highlighting active mixing beyond surface influences.

At the eddy's periphery, where SUW, GCW, and CSWr interact, ϵ is structured into layers of weak ($O\left(10^{-11}\right)$ W kg^{-1}) and high ($O\left(10^{-8}\right)$ W kg^{-1}) intensity, directly overlaying the spice and oxygen anomaly layers (Figures 1f and 1g). In these layers, temperature and salinity gradients are compensated in terms of their impact on density (see Figures S4 and S5 in Supporting Information S1), which is typical of water intrusions or layering as described in Meunier et al. (2019). Molodtsov et al. (2020) suggested the layers were double-diffusive, with a layer of diffusive convection surrounded by salt-fingering favorable environment (Figure 2h). Elevated ϵ and χ values in these layers (Figures 2a–2c) emphasize a turbulent region where thermal mixing plays a significant role, with associated Re_b values remaining below 10. The origin of the turbulence has been investigated using glider-observed spice spectra (Figure S6 in Supporting Information S1). The averaged spice spectral slope of $k^{-2.2}$ at high wavenumbers (3–30 km) is flatter than the typical k^{-3} enstrophy cascade, indicating that submesoscale processes primarily influence spice distribution in the LCR, consistent with Meunier et al. (2019). We analyzed the geostrophic Richardson number and potential vorticity using glider (not shown) and shipboard data, finding no significant evidence for conditions conductive to symmetric instabilities ($PV * f < 0$; Hoskins (1974)). These findings are in agreement with Pérez et al. (2022), who noted that such instabilities are significant in the surface boundary layer, at the periphery of the eddy, rather than in the 100–200 m depth range where the layering is observed. While the glider's alignment along the current likely underestimates the magnitude of geostrophic

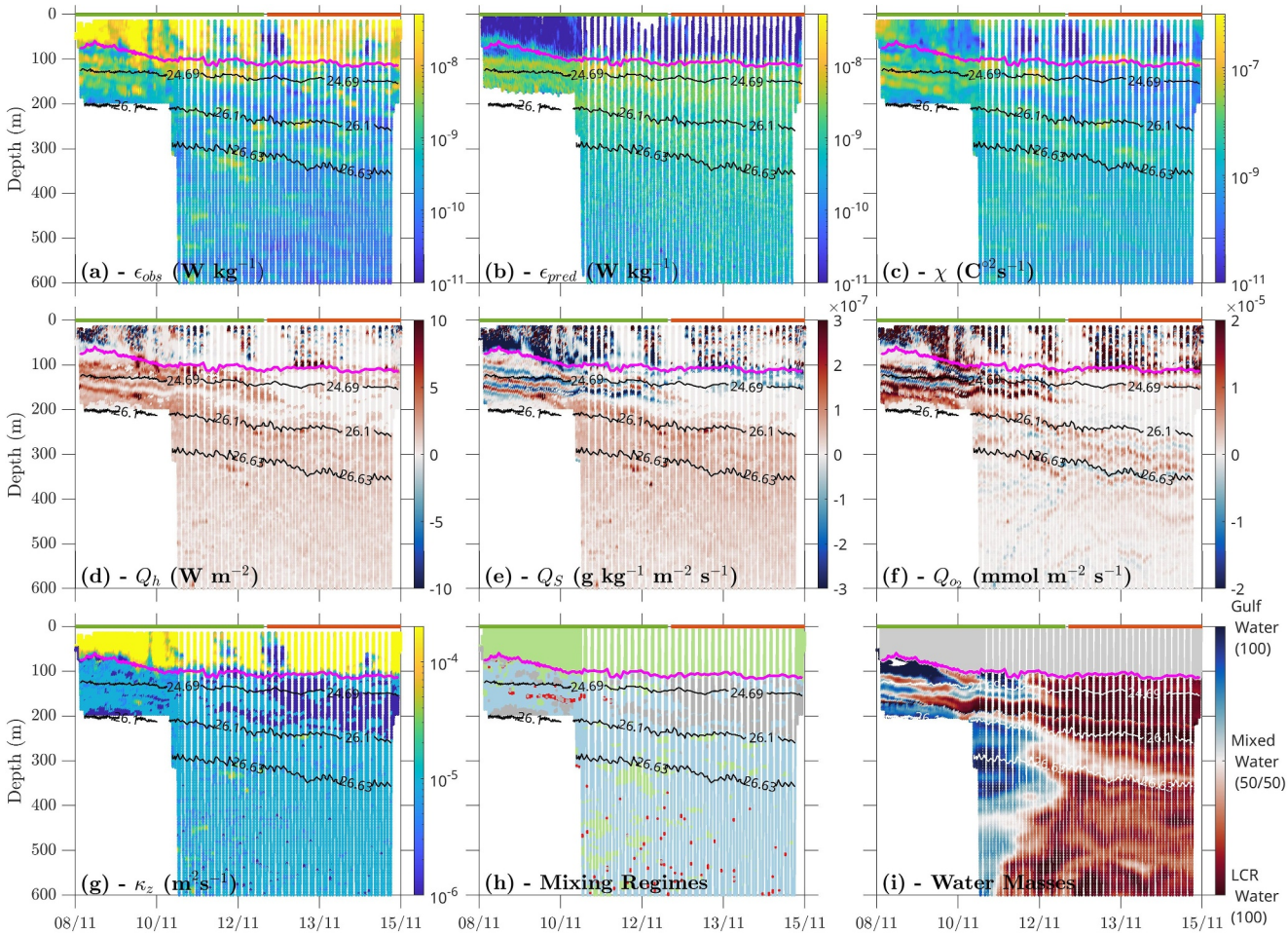

Figure 2. Glider azimuthal section showing: (a) the dissipation rates of turbulent kinetic energy from microstucture; (b) same as (a) but parameterized from Middleton et al. (2021)'s method; (c) the rate of destruction of temperature variance (d), (e), (f) vertical turbulent fluxes of heat, salt, and oxygen, respectively; (g) eddy diffusivity; (h) mixing regimes based on the buoyancy Reynolds number and the density ratio, with shear-driven mixing in green, double-convection in red, salt-finger in blue, and areas of no mixing in gray; and (i) water mass transformation expressed as percentages of LCR's and Gulf's waters. The green and orange lines at the top of each panel denote the eddy's periphery and center, respectively. Additionally, the magenta and black lines represent the mixed-layer depth and isopycnes, respectively.

vertical shear, shipboard measurements using CTD/L-ADCP confirm the results, that is, Richardson number above 1 below the mixed layer and positive potential vorticity driven by the stratification within the thermocline (Figure S7 in Supporting Information S1). We suggest, based on the work of Meunier et al. (2019), that the structures we observe are primarily formed by baroclinic instabilities driven by vertical shear, with layers subsequently tilted and deformed by submesoscale horizontal stirring. In the rest of the text, we investigate the mechanisms responsible for their dissipation.

Both shear and DDC are involved in the eddy's mixing (Figure 2h). Double-diffusive convection in the ocean is commonly characterized by staircase structures (Shibley & Timmermans, 2019). However, high-resolution temperature profiles from the glider thermistor reveal indistinct thermohaline staircases (Figure S5 in Supporting Information S1). Previous studies (Guthrie et al., 2017; Rippeth et al., 2015; Shibley & Timmermans, 2019), suggest that elevated ε reduces the presence of these structures. The double-diffusive intrusions at the eddy periphery with ε of $O(10^{-8})$ W kg^{-1}, could explain their absence. In deeper regions (>200 m), where intrusions are not observed, the internal waves shear could be responsible for the observed mixing, as found in similar mesoscale anticyclonic structures in the North Atlantic subtropical gyre and the GoM (Fernández-Castro et al., 2020; Martínez-Marrero et al., 2019; Pallàs-Sanz et al., 2016), especially at the eddy center where vertical shear of the eddy's azimuthal velocity is expected to be very weak, yielding little to no stirring.

19448007, 2024, 23, Downloaded from https://agupubs.onlinelibrary.wiley.com/doi/10.1029/2024GL110845 by Ifremer Centre Bretagne Blp, Wiley Online Library on [09/12/2024]. See the Terms and Conditions (https://onlinelibrary.wiley.com/terms-and-conditions) on Wiley Online Library for rules of use; OA articles are governed by the applicable Creative Commons License

10.1029/2024GL110845

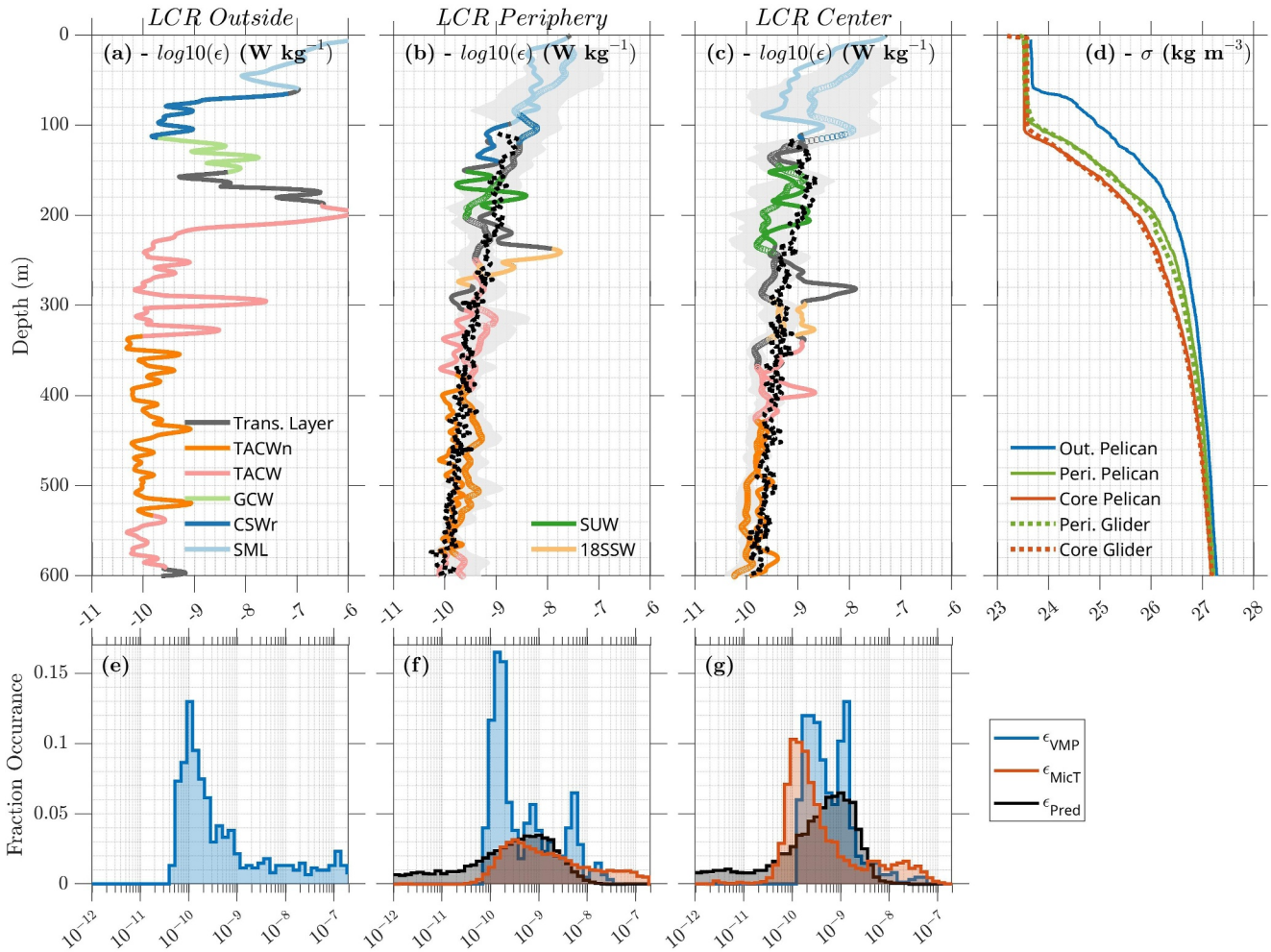

Figure 3. (a), (b), (c) Averaged profiles of turbulent dissipation rates: solid lines for vertical microstructure profiler measurements collected from RV Pelican, colored dots for glider microstructure observations, and black dots for parameterized estimates from double-diffusive convection (Middleton et al., 2021), across eddy periphery and center. Shaded areas in plots (b) and (c) represent the spatio-temporal variability of mixing observed by the Seaglider. Colors correspond to the water masses characterized in Figure 1h. (d) Profiles of density anomaly sorted by eddy location (Out. for outside, Peri. for periphery) and compared between the different platforms (RV Pelican vs. glider) (e), (f), (g) Log-histograms comparing predicted dissipation rates (ε_{Pred}) with observed rates from glider microstructure (ε_{MicT}) and vertical profiler (ε_{VMP}), covering areas outside the eddy (e), its periphery (f), and center (g), respectively.

To examine the spatial variability of ε within the LCR, we compared averaged glider turbulence observations and vertical microstructure profiles from the eddy's northeastern and western flanks, respectively (Figure 3). Over 80% of ε estimates from the vertical profiler fall within the range of background variability observed by the glider-ε estimates (Figures 3b and 3c), suggesting relatively similar conditions, despite the spatio-temporal heterogeneity of fine-scale mixing. However, the averaged glider-based ε estimates fail to capture ε maximum from the vertical profiler. At the eddy's periphery, enhanced vertical profiler's ε of $O(10^{-9})$ W kg^{-1} is observed where SUW is found around 180 m depth (Figure 3b). At this depth, spice anomaly layers with opposite signs are observed from CTD casts (Figure 1d), indicating it might be the same process (layering) observed by the glider (Figure 2a). ε maxima, from the vertical profiler, deeper than 200 m at both eddy's periphery and center, are associated with high Re_b (~100) (Figure S8 in Supporting Information S1), indicating shear-driven mixing likely due to internal wave breaking.

3.3. Turbulent Drivers of Water Masses Transformation

The optimal multiparameter analysis assesses the contributions of LCR's and Gulf's waters in each glider sample, revealing the significance of the LCR's periphery in the water mass transformation (Figure 2i). Layering consists

19448007, 2024, 23, Downloaded from https://agupubs.onlinelibrary.wiley.com/doi/10.1029/2024GL110845 by Ifremer Centre Bretagne Blp, Wiley Online Library on [09/12/2024]. See the Terms and Conditions (https://onlinelibrary.wiley.com/terms-and-conditions) on Wiley Online Library for rules of use; OA articles are governed by the applicable Creative Commons License

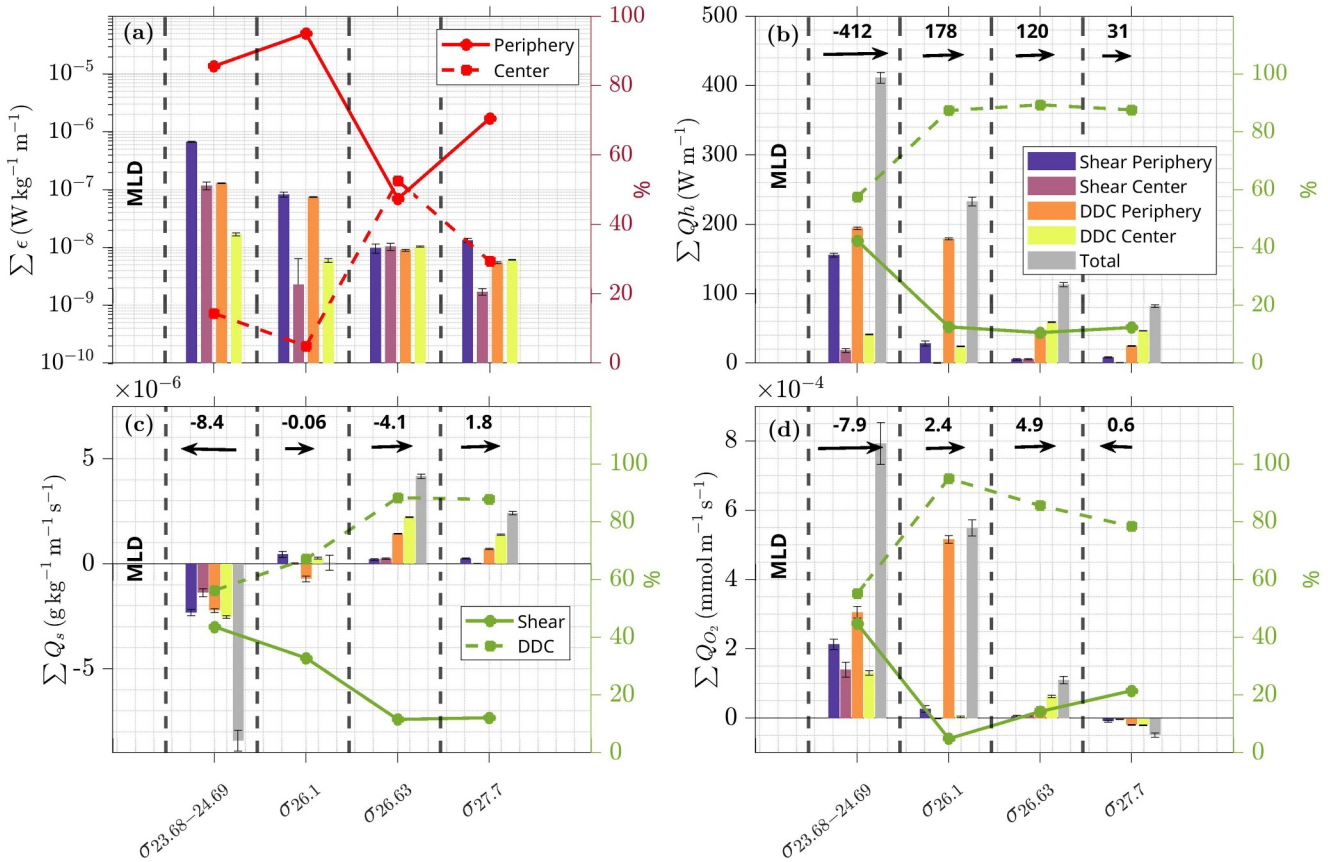

Figure 4. Contribution of (a) dissipation rates and (b), (c), (d) vertical turbulent fluxes of heat, salt, and oxygen, respectively, segmented by isopycnal layers, based on water mass distribution in the LCR (Figure 1h). They are categorized by eddy location and mixing nature: shear versus double-diffusive convection (DDC) (bar color). Relative contributions in each isopycnal layer are shown in % (red and green lines), with net turbulent fluxes changes (±) and their directions, downward (upward) fluxes are positive (negative). Vertical fluxes are normalized according to the thickness of each isopycnal layer.

in a stacking of thin layers of salty SUW alternating with thin layers of GCW. This process, driven by mesoscale azimuthal perturbations, reduces the vertical scale of thermohaline intrusions (~15–80 m) (Meunier et al., 2019). At these scales, DDC can induce statically unstable layers even at low buoyancy Reynolds numbers (Figure S8 in Supporting Information S1), enhancing the turbulent fluxes (Figures 2d–2f), and leading to the formation of well-mixed transition layers (Figure 2i). Additional well-mixed regions are observed: (a) between the LCR's periphery and core below 200 m, and (b) beneath the SUW core in the eddy's center (~300 m) where oxygen-rich 18SSW water is found (Figure 1h). Both mixed water columns closely match with increased ϵ (Figure 2a), which is induced by a mixture of shear-driven and DDC mixing (Figure 2h).

Ultimately, watermass properties are irreversibly mixed at the dissipative scale. Figure 4 illustrates the contribution of different turbulent processes in vertical turbulent fluxes of heat, salt, and oxygen, across the isopycnal layers displayed in Figure 1b. Vertical fluxes are normalized according to the thickness of each isopycnal layer, allowing for comparison between layers. Although DDC conditions are prevalent in 70% of cases (Figure 2h), shear-driven mixing is the major contributor to dissipation within the LCR, accounting in average for 78% of observed ϵ (Figure 4a). Additionally, 85% of the observed dissipation is localized in the eddy's periphery, highlighting its critical role in transforming water masses, as shown in Figure 2i. While shear-driven mixing dominates in terms of dissipation, DDC accounts in average for ~70% of the vertical turbulent fluxes of heat, salt, and oxygen (Figure 4), because of its ability to convert potential energy into TKE, for example, $\Gamma = -1$, indicating that the effective diffusivity is underestimated by $\Gamma = 0.2$.

The ability of DDC to force turbulence at low Re_b can be assessed in the LCR by comparing the magnitudes and patterns of the observed average dissipation rate, to the predicted dissipation rate from double-diffusive

19448007, 2024, 23, Downloaded from https://agupubs.onlinelibrary.wiley.com/doi/10.1029/2024GL110845 by Ifremer Centre Bretagne Blp, Wiley Online Library on [09/12/2024]. See the Terms and Conditions (https://onlinelibrary.wiley.com/terms-and-conditions) on Wiley Online Library for rules of use; OA articles are governed by the applicable Creative Commons License

convection parameterized following Middleton et al. (2021) (Figures 3b and 3c, black dots). Histograms of the estimated and observed dissipation rates from microstructure show similar distribution in the eddy's periphery (Figure 3f), and reproduce 82% of the observations within an order of magnitude in the layering area. However, in the eddy center, results show that the parameterized dissipation rate due to DDC is overestimated compared to observations (Figure 3g). The DDC parameterization assumes a k^{-1} slope for the variance spectrum of spice, which is likely an overestimate in this region due to the weak stirring, leading to the overestimation of mixing within the SUW core (Figure 2b), as in Fine et al. (2022). Whilst the density ratio Figure 2h is a mixture of doubly stable, salt fingering favorable and diffusive convection favorable, the buoyancy Reynolds number is skewed to the left, that is, <10 (Figure S8 in Supporting Information S1), suggesting that in most cases, stratification suppresses shear-production. Vertical fluxes are therefore largely driven by DDC triggering turbulence in the LCR.

3.4. Diapycnal Turbulent Fluxes

The vertical fluxes of heat, salt, and oxygen between the isopycnals layers, based on the water mass distribution in the LCR are shown in Figure 4. Our analysis reveals that vertical fluxes of heat and oxygen are predominantly downward (positive), except in the deeper region where oxygen fluxes are upward (negative, Figures 4b and 4d). Below the 24.69 kg m^{-3} isopycnal, the water column warms and gains oxygen, as indicated by the positive net fluxes (Figures 4b and 4d). In contrast, the layer just below the mixed layer shows the opposite, with cooling (-412 W m^{-1}) and deoxygenation (-7.9 $\times$ 10^{-4} mmol m^{-1} s^{-1}) due to its interaction with surface forcings. Vertical salt fluxes exhibit a more complex pattern with a divergence around the 24.69–26.1 kg m^{-3} isopycnal, where thermohaline intrusions are found (Figure 2a). The layer above has a net upward flux, while the layer below has a net downward flux (Figure 4c). Thermohaline intrusions lead to a net downward salt flux of -0.06 $\times$ 10^{-6} g kg^{-1} m^{-1} s^{-1}, where the SUW is found. Therefore, this double-diffusive process contributes to the erosion of the subsurface maximum salinity of the SUW. However, the finer-scale complexity of tracer gradients, particularly in the layering, could influence net vertical fluxes (Carpenter et al., 2022). While these smaller-scale vertical fluxes might cancel each other out (at the order of meter), our approach focuses on larger vertical scales between isopycnal layers of ≈100 m, capturing the broader transformation processes throughout the eddy.

Meunier et al. (2020) suggests that lateral mixing at submesoscale scale (<25 km) is an important process for LCR's heat dispersion. Assuming the intrusions are in quasi-steady state, vertical production of temperature variance must be balanced by large-scale horizontal production of variance. Following B. R. Ruddick et al. (2010) and Hebert et al. (1990), we estimated the isopycnal diffusivity resulting from advection along intrusions for heat, $\kappa_{T\,DDC}^{sides} = \kappa_T(\delta T/\delta z)^2/(\delta T/\delta x)^2$, and salt, $\kappa_{S\,DDC}^{sides} = \kappa_S(\delta S/\delta z)^2/(\delta S/\delta x)^2$, where κ_T and κ_S were derived from Equations 8 and 9, respectively. In the thermohaline intrusions, the averaged horizontal heat, $-\rho c_p \kappa_{T\,DDC}^{sides}\langle \delta T/\delta x\rangle$, and salt, $(1/1000)\left(-\rho \kappa_{S\,DDC}^{sides}\langle \delta S/\delta x\rangle\right)$, fluxes are approximately 200 W m^{-2} and 5 $\times$ 10^{-6} g kg^{-1} m^{-1} s^{-1}, respectively. These values are two and three orders of magnitude higher than the averaged vertical fluxes, which are around 0.5 W m^{-2} for heat and 6 $\times$ 10^{-9} g kg^{-1} m^{-1} s^{-1} for salt, consistent with observations in similar finescale structures (Fine et al., 2018; Molodtsov et al., 2020). As shown in Figure 2a, the layering involves alternating zones of high and low turbulence. Within these low-turbulence layers, significant thermal variance is generated by lateral variability in water masses, as described by Carpenter et al. (2022). This process enhances mixing even in weakly turbulent conditions by creating fine-scale structures that drive horizontal fluxes, contributing to the transformation of Subtropical Underwater into Gulf Common Water.

4. Summary and Discussion

This observational study provides quantitative estimates of the turbulent processes within the LCR "Yazoo", and their influence on turbulent fluxes and water mass transformation. Our results indicate that shear-driven mixing, does not account for the total heat, salt and oxygen fluxes, and that double-diffusive convection needs to be considered as a key process to explain these turbulent fluxes and water mass transformation.

Through detailed microstructure measurements, we captured the processes driving turbulent mixing. Below the mixed layer, we observed enhanced dissipation rates ($O(10^{-8})$ W kg^{-1}) at the eddy's periphery, beneath its core, and deeper within the eddy. We have shown that DDC can explain the dissipation at the eddy's edges,

19448007, 2024, 23, Downloaded from https://agupubs.onlinelibrary.wiley.com/doi/10.1029/2024GL110845 by Ifremer Centre Bretagne Blp, Wiley Online Library on [09/12/2024]. See the Terms and Conditions (https://onlinelibrary.wiley.com/terms-and-conditions) on Wiley Online Library for rules of use; OA articles are governed by the applicable Creative Commons License

19448007, 2024, 23, Downloaded from https://agupubs.onlinelibrary.wiley.com/doi/10.1029/2024GL110845 by Ifremer Centre Bretagne Blp, Wiley Online Library on [09/12/2024]. See the Terms and Conditions (https://onlinelibrary.wiley.com/terms-and-conditions) on Wiley Online Library for rules of use; OA articles are governed by the applicable Creative Commons License

but not at depth, where it is likely due to internal wave breaking, as observed in various studies (Fernández-Castro et al., 2020; Martínez-Marrero et al., 2019; Pallàs-Sanz et al., 2016). Anticyclonic eddies as LCRs have been shown to induce DDC around their edges in the Arctic (Fine et al., 2018), Mediterranean (Armi et al., 1989; Tokos & Rossby, 1991), Gulf Stream rings (B. Ruddick & Bennett, 1985; Schmitt et al., 1986), and the Gulf of Mexico (Meunier et al., 2019; Molodtsov et al., 2020). Additionally, the eddy's periphery emerges as a hotspot responsible for 85% of the total dissipation (Figure 4a), highlighting the need for models to accurately capture this narrow band of few kilometers thick to effectively resolve the processes driving the mesoscale eddy decay.

This study also suggests that a possible mechanism of submesoscale stirring of spice leads to DDC, which is a key process in the route toward transformation of SUW into GCW. We also showed the importance of lateral mixing (few times larger than vertical), associated with thermohaline intrusions, in diffusing the LCR's heat and salt, as suggested in Meunier et al. (2019, 2020). These results challenge the perspective that GCW formation results principally from the vertical mixing of TACW and CSWr (Cervantes-Díaz et al., 2022), suggesting instead that SUW significantly influences GCW formation. Although our observations focus on a single LCR, layering appears to be a recurrent process (Meunier et al., 2019; Molodtsov et al., 2020), and therefore highly relevant for water mass transformation in the GoM.

One important result of this study is the seemingly secondary role played by shear-driven mixing in the eddy's water mass exchanges. Although on average, shear mixing corresponds to ∼80% of the total dissipation—mainly due to the intense mixing in the subsurface layer interacting directly with the mixed layer depth (Figure 4a)—it accounts for only a third of vertical fluxes within the eddy. This disparity is attributed to the prevalence of DDC conductive conditions (∼70% of occurrence), where all potential energy is converted into TKE, a mechanism contrasting sharply with shear-driven mixing (Inoue et al., 2007; Laurent & Schmitt, 1999). To verify that DDC is sufficiently strong to control water mass exchanges within the LCR, we applied the parameterization of Middleton et al. (2021) to estimate ε due to double-diffusion. While this method underestimated ε in the high shear regions, it reproduced the enhanced ε observed in the region of enhanced submesoscale stirring on the LCR periphery, capturing 82% of the observations within an order of magnitude. These findings show that the submesoscale stirring of compensated thermohaline variance (spice) along isopycnals may play an essential role in water mass transformation. Using the classical Osborn (1980) model, with a $\Gamma = 0.2$ suited for shear-driven mixing, leads to a 42% underestimation of vertical turbulent fluxes. However, adjusting $\Gamma = -1$ to capture DDC dynamics (Laurent & Schmitt, 1999) gives significantly larger rates of vertical turbulent fluxes, hence water mass transformation.

We have shown that double-diffusive convection, favored by submesoscale stirring, is potentially important in water mass transformation in the Gulf of Mexico. However, the effect of DDC on water mass transformation has not been quantified on a global scale. Given that LCRs are the principal source of water mass variability in the Gulf of Mexico (Portela et al., 2018), an ongoing study is employing both internal-wave (Whalen et al., 2015) and double-diffusive (Middleton et al., 2021) parameterizations to estimate ε across all LCRs identified by the 30 missions of the glider group since 2016. This effort will aim at enhancing our understanding of warm-core rings' role in tracer transport and diffusion at the basin scale.

Data Availability Statement

The processed data used in this article needed to understand, evaluate, and build upon the reported research are available in the repository of the Group of Monitoring the Ocean (GMOG). The database is called TurbulentPBE and can accessed using the link https://gliders.cicese.mx/databases/TurbulentPBE. Will be required to disclose (a) name, (b) last name, (c) e-mail address, (d) name of the institution, and (e) specify how the TurbulentPBE will be used. GMOG-CICESE will authorize the access and will email to the user a username and password to download the TurbulentPBE database. Anonymous reviewers have granted access to the data, credentials are not required. The TurbulentPBE database can be licensed for non-commerical use, and it is prohibited to share it with third parties, as well as to profit or sell products derived from it. We utilized the software developed by Scheifele et al. (2018) for calculating turbulent kinetic energy dissipation rates, (https://github.com/bscheife/turbulence_temperature [Software]).

Acknowledgments
This work and the postdoctoral fellowship of the corresponding author were supported by the project "Phytoplankton Blooms in a Loop Current Eddy" (FORDECYT-PRONACES/1327709/2020) from Consejo Nacional de Humanidades, Ciencias y Tecnologías de México (CONAHCyT). We acknowledge the contribution of all the staff of Grupo de Monitoreo Oceanográfico con Gliders (GMOG) at the Centro de Investigación Científica y de Educación Superior de Ensenada, Baja California (CICESE), specially to Adrian Villicaña for piloting underwater gliders, and to Johanna Saavedra and Eliot Aranda Gonzalez for data management. We are also grateful to the Dr. Anthony Bosse and the Rockland Scientific team, specially the Dr. Anneke Ten Doeschate and Evan Cervelli for their support to process glider-MicroPod data. Angel Ruiz-Angulo would like to acknowledge the support of the UI's Research Fund, RSJ2022-90347. Finally, we extend our sincere thanks to Dr. Jeff Carpenter, the anonymous reviewer, and the journal editor for their constructive and thoughtful comments and suggestions.

References

Armi, L., Hebert, D., Oakey, N., Price, J. F., Richardson, P. L., Rossby, H. T., & Ruddick, B. (1989). Two years in the life of a mediterranean salt lens. *Journal of Physical Oceanography*, *19*(3), 354–370. https://doi.org/10.1175/1520-0485(1989)019<0354:tyitlo>2.0.co;2

Batchelor, G. K. (1959). Small-scale variation of convected quantities like temperature in turbulent fluid part 1. general discussion and the case of small conductivity. *Journal of Fluid Mechanics*, *5*(1), 113–133. https://doi.org/10.1017/s002211205900009x

Bebieva, Y., & Timmermans, M.-L. (2016). An examination of double-diffusive processes in a mesoscale eddy in the arctic ocean. *Journal of Geophysical Research: Oceans*, *121*(1), 457–475. https://doi.org/10.1002/2015jc011105

Bouffard, D., & Boegman, L. (2013). A diapycnal diffusivity model for stratified environmental flows. *Dynamics of Atmospheres and Oceans*, *61*, 14–34. https://doi.org/10.1016/j.dynatmoce.2013.02.002

Brannigan, L. (2016). Intense submesoscale upwelling in anticyclonic eddies. *Geophysical Research Letters*, *43*(7), 3360–3369. https://doi.org/10.1002/2016gl067926

Carpenter, J. R., Waterman, S., & Scheifele, B. (2022). Enhanced mixing of heat in the arctic ocean halocline in weakly turbulent conditions. *Geophysical Research Letters*, *49*(24), e2022GL100450. https://doi.org/10.1029/2022gl100450

Cervantes-Díaz, G. Y., Hernández-Ayón, J. M., Zirino, A., Herzka, S. Z., Camacho-Ibar, V., Norzagaray, O., et al. (2022). Understanding upper water mass dynamics in the gulf of Mexico by linking physical and biogeochemical features. *Journal of Marine Systems*, *225*, 103647. https://doi.org/10.1016/j.jmarsys.2021.103647

Chaigneau, A., Gizolme, A., & Grados, C. (2008). Mesoscale eddies off Peru in altimeter records: Identification algorithms and eddy spatio-temporal patterns. *Progress in Oceanography*, *79*(2–4), 106–119. https://doi.org/10.1016/j.pocean.2008.10.013

Damien, P., Sheinbaum, J., Pasqueron de Fommervault, O., Jouanno, J., Linacre, L., & Duteil, O. (2021). Do loop current eddies stimulate productivity in the gulf of Mexico? *Biogeosciences*, *18*(14), 4281–4303. https://doi.org/10.5194/bg-18-4281-2021

Fernández-Castro, B., Evans, D. G., Frajka-Williams, E., Vic, C., & Naveira-Garabato, A. C. (2020). Breaking of internal waves and turbulent dissipation in an anticyclonic mode water eddy. *Journal of Physical Oceanography*, *50*(7), 1893–1914. https://doi.org/10.1175/JPO-D-19-0168.1

Ferrell, R. T., & Himmelblau, D. M. (1967). Diffusion coefficients of nitrogen and oxygen in water. *Journal of Chemical and Engineering Data*, *12*(1), 111–115.

Fine, E. C., MacKinnon, J. A., Alford, M. H., & Mickett, J. B. (2018). Microstructure observations of turbulent heat fluxes in a warm-core Canada basin eddy. *Journal of Physical Oceanography*, *48*(10), 2397–2418. https://doi.org/10.1175/jpo-d-18-0028.1

Fine, E. C., MacKinnon, J. A., Alford, M. H., Middleton, L., Taylor, J., Mickett, J. B., et al. (2022). Double diffusion, shear instabilities, and heat impacts of a pacific summer water intrusion in the beaufort sea. *Journal of Physical Oceanography*, *52*(2), 189–203. https://doi.org/10.1175/jpo-d-21-0074.1

Frajka-Williams, E., Brearley, J. A., Nash, J. D., & Whalen, C. B. (2022). New technological frontiers in ocean mixing. *Ocean mixing*, 345–361. Elsevier.

Gargett, A. E. (1988). The scaling of turbulence in the presence of stable stratification. *Journal of Geophysical Research*, *93*(C5), 5021–5036. https://doi.org/10.1029/jc093ic05p05021

Guthrie, J. D., Fer, I., & Morison, J. H. (2017). Thermohaline staircases in the a mundsen b asin: Possible disruption by shear and mixing. *Journal of Geophysical Research: Oceans*, *122*(10), 7767–7782. https://doi.org/10.1002/2017jc012993

Hamilton, J. M., Lewis, M. R., & Ruddick, B. R. (1989). Vertical fluxes of nitrate associated with salt fingers in the world's oceans. *Journal of Geophysical Research*, *94*(C2), 2137–2145. https://doi.org/10.1029/jc094ic02p02137

Hamilton, P., Leben, R., Bower, A., Furey, H., & Pérez-Brunius, P. (2018). Hydrography of the gulf of Mexico using autonomous floats. *Journal of Physical Oceanography*, *48*(4), 773–794. https://doi.org/10.1175/jpo-d-17-0205.1

Hebert, D., Oakey, N., & Ruddick, B. (1990). Evolution of a mediterranean salt lens: Scalar properties. *Journal of Physical Oceanography*, *20*(9), 1468–1483. https://doi.org/10.1175/1520-0485(1990)020<1468:eoamsl>2.0.co;2

Herring, H. (2010). Gulf of Mexico hydrographic climatology and method of synthesizing subsurface profiles from the satellite sea surface height anomaly. *Dynalysis of Princeton*.

Hoskins, B. (1974). The role of potential vorticity in symmetric stability and instability. *Quarterly Journal of the Royal Meteorological Society*, *100*(425), 480–482. https://doi.org/10.1002/qj.49710042520

Inoue, R., Yamazaki, H., Wolk, F., Kono, T., & Yoshida, J. (2007). An estimation of buoyancy flux for a mixture of turbulence and double diffusion. *Journal of Physical Oceanography*, *37*(3), 611–624. https://doi.org/10.1175/jpo2996.1

Ivey, G., Winters, K., & Koseff, J. (2008). Density stratification, turbulence, but how much mixing? *Annual Review of Fluid Mechanics*, *40*(1), 169–184. https://doi.org/10.1146/annurev.fluid.39.050905.110314

Jackson, P. R., & Rehmann, C. R. (2014). Experiments on differential scalar mixing in turbulence in a sheared, stratified flow. *Journal of Physical Oceanography*, *44*(10), 2661–2680. https://doi.org/10.1175/jpo-d-14-0027.1

Jaimes, B., Shay, L. K., & Brewster, J. K. (2016). Observed air-sea interactions in tropical cyclone isaac over loop current mesoscale eddy features. *Dynamics of Atmospheres and Oceans*, *76*, 306–324. https://doi.org/10.1016/j.dynatmoce.2016.03.001

John, E. B., Balaguru, K., Leung, L. R., Foltz, G. R., Hetland, R. D., & Hagos, S. M. (2023). Intensification of hurricane sally (2020) over the Mississippi river plume. *Weather and Forecasting*, *38*(8), 1391–1404. https://doi.org/10.1175/waf-d-22-0191.1

Kunze, E. (2003). A review of oceanic salt-fingering theory. *Progress in Oceanography*, *56*(3–4), 399–417. https://doi.org/10.1016/s0079-6611(03)00027-2

Laurent, L. S., & Schmitt, R. W. (1999). The contribution of salt fingers to vertical mixing in the north atlantic tracer release experiment. *Journal of Physical Oceanography*, *29*(7), 1404–1424. https://doi.org/10.1175/1520-0485(1999)029<1404:tcosft>2.0.co;2

Linacre, L., Durazo, R., Camacho-Ibar, V., Selph, K., Lara-Lara, J., Mirabal-Gómez, U., et al. (2019). Picoplankton carbon biomass assessments and distribution of prochlorococcus ecotypes linked to loop current eddies during summer in the southern gulf of Mexico. *Journal of Geophysical Research: Oceans*, *124*(11), 8342–8359. https://doi.org/10.1029/2019jc015103

Martínez-Marrero, A., Barceló-Llull, B., Pallàs-Sanz, E., Aguiar-González, B., Estrada-Allis, S. N., Gordo, C., et al. (2019). Near-inertial wave trapping near the base of an anticyclonic mesoscale eddy under normal atmospheric conditions. *Journal of Geophysical Research: Oceans*, *124*(11), 8455–8467. https://doi.org/10.1029/2019jc015168

McDougall, T. J., & Barker, P. M. (2011). Getting started with teos-10 and the Gibbs seawater (gsw) oceanographic toolbox. *Scor/Iapso WG*, *127*(532), 1–28.

Meunier, T., Bower, A., Pérez-Brunius, P., Graef, F., & Mahadevan, A. (2024). The energy decay of warm-core eddies in the gulf of Mexico. *Geophysical Research Letters*, *51*(1), e2023GL106246. https://doi.org/10.1029/2023gl106246

19448007, 2024, 23, Downloaded from https://agupubs.onlinelibrary.wiley.com/doi/10.1029/2024GL110845 by Ifremer Centre Bretagne Blp, Wiley Online Library on [09/12/2024]. See the Terms and Conditions (https://onlinelibrary.wiley.com/terms-and-conditions) on Wiley Online Library for rules of use; OA articles are governed by the applicable Creative Commons License

Meunier, T., Ménesguen, C., Schopp, R., & Le Gentil, S. (2015). Tracer stirring around a meddy: The formation of layering. *Journal of Physical Oceanography*, *45*(2), 407–423. https://doi.org/10.1175/jpo-d-14-0061.1

Meunier, T., Pallás-Sanz, E., Tenreiro, M., Portela, E., Ochoa, J., Ruiz-Angulo, A., & Cusí, S. (2018). The vertical structure of a loop current eddy. *Journal of Geophysical Research: Oceans*, *123*(9), 6070–6090. https://doi.org/10.1029/2018jc013801

Meunier, T., Sanz, E. P., Tenreiro, M., Ochoa, J., Angulo, A. R., & Buckingham, C. (2019). Observations of layering under a warm-core ring in the gulf of Mexico. *Journal of Physical Oceanography*, *49*(12), 3145–3162. https://doi.org/10.1175/jpo-d-18-0138.1

Meunier, T., Sheinbaum, J., Pallàs-Sanz, E., Tenreiro, M., Ochoa, J., Ruiz-Angulo, A., et al. (2020). Heat content anomaly and decay of warm-core rings: The case of the gulf of Mexico. *Geophysical Research Letters*, *47*(3), e2019GL085600. https://doi.org/10.1029/2019gl085600

Middleton, L., Fine, E., MacKinnon, J., Alford, M., & Taylor, J. (2021). Estimating dissipation rates associated with double diffusion. *Geophysical Research Letters*, *48*(15), e2021GL092779. https://doi.org/10.1029/2021gl092779

Molodtsov, S., Anis, A., Amon, R., & Perez-Brunius, P. (2020). Turbulent mixing in a loop current eddy from glider-based microstructure observations. *Geophysical Research Letters*, *47*(14), e2020GL088033. https://doi.org/10.1029/2020gl088033

Monterey, G. I., & Levitus, S. (1997). Seasonal variability of mixed layer depth for the world ocean.

Osborn, T. R. (1980). Estimates of the local rate of vertical diffusion from dissipation measurements. *Journal of Physical Oceanography*, *10*(1), 83–89. https://doi.org/10.1175/1520-0485(1980)010<0083:eotlro>2.0.co;2

Osborn, T. R., & Cox, C. S. (1972). Oceanic fine structure. *Geophysical Fluid Dynamics*, *3*(4), 321–345. https://doi.org/10.1080/03091927208236085

Oyabu, R., Yasuda, I., & Sasaki, Y. (2023). Large-scale distribution and variations of active salt-finger double-diffusion in the western north pacific. *Journal of Physical Oceanography*, *53*(8), 2013–2027. https://doi.org/10.1175/jpo-d-22-0244.1

Pallàs-Sanz, E., Candela, J., Sheinbaum, J., & Ochoa, J. (2016). Mooring observations of the near-inertial wave wake of hurricane ida (2009). *Dynamics of Atmospheres and Oceans*, *76*, 325–344. https://doi.org/10.1016/j.dynatmoce.2016.05.003

Pérez, J., Pallàs-Sanz, E., Tenreiro, M., Meunier, T., Jouanno, J., & Ruiz-Angulo, A. (2022). Overturning instabilities across a warm core ring from glider observations. *Journal of Geophysical Research: Oceans*, *127*(4), e2021JC017527. https://doi.org/10.1029/2021jc017527

Peterson, A. K., & Fer, I. (2014). Dissipation measurements using temperature microstructure from an underwater glider. *Methods in Oceanography*, *10*, 44–69. https://doi.org/10.1016/j.mio.2014.05.002

Pollard, R. T., Rhines, P. B., & Thompson, R. O. (1973). The deepening of the wind-mixed layer. *Geophysical Fluid Dynamics*, *4*(4), 381–404. https://doi.org/10.1080/03091927208236105

Portela, E., Tenreiro, M., Pallàs-Sanz, E., Meunier, T., Ruiz-Angulo, A., Sosa-Gutiérrez, R., & Cusí, S. (2018). Hydrography of the central and western gulf of Mexico. *Journal of Geophysical Research: Oceans*, *123*(8), 5134–5149. https://doi.org/10.1029/2018jc013813

Rippeth, T. P., Lincoln, B. J., Lenn, Y.-D., Green, J. M., Sundfjord, A., & Bacon, S. (2015). Tide-mediated warming of arctic halocline by atlantic heat fluxes over rough topography. *Nature Geoscience*, *8*(3), 191–194. https://doi.org/10.1038/ngeo2350

Ruddick, B., Anis, A., & Thompson, K. (2000). Maximum likelihood spectral fitting: The batchelor spectrum. *Journal of Atmospheric and Oceanic Technology*, *17*(11), 1541–1555. https://doi.org/10.1175/1520-0426(2000)017<1541:mlsftb>2.0.co;2

Ruddick, B., & Richards, K. (2003). Oceanic thermohaline intrusions: Observations. *Progress in Oceanography*, *56*(3–4), 499–527. https://doi.org/10.1016/s0079-6611(03)00028-4

Ruddick, B. R., & Bennett, A. S. (1985). Fine structure and mixing at the edge of a warm core ring. *Journal of Geophysical Research*, *90*(C5), 8943–8951. https://doi.org/10.1029/jc090ic05p08943

Ruddick, B. R., Oakey, N. S., & Hebert, D. (2010). Measuring lateral heat flux across a thermohaline front: A model and observational test. *Journal of Marine Research*, *68*(3–4), 523–539. https://doi.org/10.1357/002224010794657146

Sanchez-Rios, A., Shearman, R. K., Lee, C. M., Simmons, H. L., St. Laurent, L., Lucas, A. J., et al. (2024). Characterization of mixing at the edge of a kuroshio intrusion into the south China sea: Analysis of thermal variance diffusivity measurements. *Journal of Physical Oceanography*, *54*(5), 1121–1142. https://doi.org/10.1175/jpo-d-23-0007.1

Scheifele, B., Waterman, S., Merckelbach, L., & Carpenter, J. R. (2018). Measuring the dissipation rate of turbulent kinetic energy in strongly stratified, low-energy environments: A case study from the arctic ocean. *Journal of Geophysical Research: Oceans*, *123*(8), 5459–5480. https://doi.org/10.1029/2017jc013731

Schmitt, R. W. (1994). Double diffusion in oceanography. *Annual Review of Fluid Mechanics*, *26*(1), 255–285. https://doi.org/10.1146/annurev.fl.26.010194.001351

Schmitt, R. W., Lueck, R. G., & Joyce, T. M. (1986). Fine-and microstructure at the edge of a warm-core ring. Deep Sea Research Part A. *Oceanographic Research Papers*, *33*(11–12), 1665–1689. https://doi.org/10.1016/0198-0149(86)90073-7

Shay, L. K., Goni, G. J., & Black, P. G. (2000). Effects of a warm oceanic feature on hurricane opal. *Monthly Weather Review*, *128*(5), 1366–1383. https://doi.org/10.1175/1520-0493(2000)128<1366:eoawof>2.0.co;2

Shcherbina, A. Y., Gregg, M. C., Alford, M. H., & Harcourt, R. R. (2009). Characterizing thermohaline intrusions in the north pacific subtropical frontal zone. *Journal of Physical Oceanography*, *39*(11), 2735–2756. https://doi.org/10.1175/2009jpo4190.1

Shibley, N., & Timmermans, M.-L. (2019). The formation of double-diffusive layers in a weakly turbulent environment. *Journal of Geophysical Research: Oceans*, *124*(3), 1445–1458. https://doi.org/10.1029/2018jc014625

Shih, L. H., Koseff, J. R., Ivey, G. N., & Ferziger, J. H. (2005). Parameterization of turbulent fluxes and scales using homogeneous sheared stably stratified turbulence simulations. *Journal of Fluid Mechanics*, *525*, 193–214. https://doi.org/10.1017/s0022112004002587

Sosa-Gutiérrez, R., Pallàs-Sanz, E., Jouanno, J., Chaigneau, A., Candela, J., & Tenreiro, M. (2020). Erosion of the subsurface salinity maximum of the loop current eddies from glider observations and a numerical model. *Journal of Geophysical Research: Oceans*, *125*(7), e2019JC015397. https://doi.org/10.1029/2019jc015397

Stillinger, D., Helland, K., & Van Atta, C. (1983). Experiments on the transition of homogeneous turbulence to internal waves in a stratified fluid. *Journal of Fluid Mechanics*, *131*(-1), 91–122. https://doi.org/10.1017/s0022112083001251

Thirion, G., Birol, F., & Jouanno, J. (2024). Loop current eddies as a possible cause of the rapid sea level rise in the gulf of Mexico. *Journal of Geophysical Research: Oceans*, *129*(3), e2023JC019764. https://doi.org/10.1029/2023jc019764

Tokos, K. S., & Rossby, T. (1991). Kinematics and dynamics of a mediterranean salt lens. *Journal of Physical Oceanography*, *21*(6), 879–892. https://doi.org/10.1175/1520-0485(1991)021<0879:kadoam>2.0.co;2

Tomczak, M. (1981). A multi-parameter extension of temperature/salinity diagram techniques for the analysis of non-isopycnal mixing. *Progress in Oceanography*, *10*(3), 147–171. https://doi.org/10.1016/0079-6611(81)90010-0

Tomczak, M. (1999). Some historical, theoretical and applied aspects of quantitative water mass analysis. *Journal of Marine Research*, *57*(2), 275–303. https://doi.org/10.1357/002224099321618227

Tomczak, M., & Large, D. G. (1989). Optimum multiparameter analysis of mixing in the thermocline of the eastern indian ocean. *Journal of Geophysical Research*, *94*(C11), 16141–16149. https://doi.org/10.1029/jc094ic11p16141

19448007, 2024, 23, Downloaded from https://agupubs.onlinelibrary.wiley.com/doi/10.1029/2024GL110845 by Ifremer Centre Bretagne Blp, Wiley Online Library on [09/12/2024]. See the Terms and Conditions (https://onlinelibrary.wiley.com/terms-and-conditions) on Wiley Online Library for rules of use; OA articles are governed by the applicable Creative Commons License

Vidal, V. M., Vidal, F. V., Hernández, A. F., Meza, E., & Zambrano, L. (1994). Winter water mass distributions in the western gulf of Mexico affected by a colliding anticyclonic ring. *Journal of Oceanography*, *50*(5), 559–588. https://doi.org/10.1007/bf02235424

Vitagliano, V., & Lyons, P. A. (1956). Diffusion coefficients for aqueous solutions of sodium chloride and barium chloride. *Journal of the American Chemical Society*, *78*(8), 1549–1552.

Washburn, L., & Käse, R. H. (1987). Double diffusion and the distribution of the density ratio in the mediterranean waterfront southeast of the azores. *Journal of Physical Oceanography*, *17*(1), 12–25. https://doi.org/10.1175/1520-0485(1987)017<0012:ddatdo>2.0.co;2

Whalen, C. B., MacKinnon, J. A., Talley, L. D., & Waterhouse, A. F. (2015). Estimating the mean diapycnal mixing using a finescale strain parameterization. *Journal of Physical Oceanography*, *45*(4), 1174–1188. https://doi.org/10.1175/jpo-d-14-0167.1

Wu, L., Rutgersson, A., & Sahlée, E. (2015). Upper-ocean mixing due to surface gravity waves. *Journal of Geophysical Research: Oceans*, *120*(12), 8210–8228. https://doi.org/10.1002/2015jc011329

Yang, Y., Verzicco, R., & Lohse, D. (2016). From convection rolls to finger convection in double-diffusive turbulence. *Proceedings of the National Academy of Sciences*, *113*(1), 69–73. https://doi.org/10.1073/pnas.1518040113

19448007, 2024, 23, Downloaded from https://agupubs.onlinelibrary.wiley.com/doi/10.1029/2024GL110845 by Ifremer Centre Bretagne Blp, Wiley Online Library on [09/12/2024]. See the Terms and Conditions (https://onlinelibrary.wiley.com/terms-and-conditions) on Wiley Online Library for rules of use; OA articles are governed by the applicable Creative Commons License